Batteries & Supercaps

Research Article
doi.org/10.1002/batt.202400493

Chemistry Europe
European Chemical Societies Publishing

www.batteries-supercaps.org

$Ti_3C_2T_x$ MXene Electrode-Electrolyte Interface Reactions at Different Stages of Charge/Discharge in Lithium and Sodium Half-Cells

Anjali V Nair,[a] Dona Susan Baji,[a] Shantikumar Nair,[a] and Dhamodaran Santhanagopalan*[a]

Energy storage technologies necessitates efficient, cost effective, and durable storage systems like Li-ion batteries (LIBs), with high energy density. Emerging 2D materials like MXenes have become significant for battery applications. Herein, titanium carbide ($Ti_3C_2T_x$) synthesized and lattice engineered via -OH surface terminations removal by thermal processing is well explained. The synthesized samples were subjected to annealing at 250 and 500 °C. All the samples were characterized using XRD, TEM, XPS, etc. Subsequently, they were tested in the half-cell configuration for both lithium and sodium ion batteries (NIBs). It is observed that the best performance for lithium-ion storage capacity was 200 mAh/g at 50 mA/g and 125 mAh/g at the same specific current for sodium-ion storage for the 500 °C processed sample. However, for both the systems the cycling stability was exceptional maintaining high retention till the end of 1000 cycles. To establish the performance, electrochemical impedance and ex situ XPS results at different voltage of 1st charge/discharge were correlated for the best sample. Thus, providing information that is unavailable in the literature on MXene-electrolyte interactions, kinetics and the chemical nature of solid-electrolyte interface layer for both lithium and sodium-ion batteries.

Introduction

In the current scenario the role of electrochemical energy systems is crucial as it offers solution to wide range of fields such as energy storage and conversion, decentralized power generation, portable power systems etc. for a cleaner and sustainable energy environment. Among the indispensable energy storage systems, batteries play dominant role in meeting the high energy demands with high energy density from hand-held electronics to huge devices since they are perpetual.[1,2] After the first commercialization in 1990s, Li-ion batteries became a primary candidate because of its high energy density and output voltages. Despite of this, increasing demands, high cost and limitation in reserves are major challenges faced by LIBs, which actually draws attention to ambient-temperature rechargeable Na-ion batteries.[3,4] Due to similar chemical properties and mechanisms with LIBs, research is going on to produce cheaper and safer NIBs.[5] Although LIBs and NIBs have resemblance, due to larger atomic radius of sodium ions, exhibit mismatches in the most known anode materials of LIBs results in insufficient interlayer spacing and volume expansion happens when sodiation/desodiation occurs.[6] Emergence of layered 2D materials after the discovery of graphene, in batteries as anode paves way to design suitable anode which possess better optical and electrochemical properties with strong-in-plane bond with atoms and weak force of interaction between layers.[7] The atomically thin 2D materials having high surface-to-volume ratio with exceptional electrical, mechanical and optical properties. Such advanced properties motivate researchers to synthesize different types of 2D materials like, transition metal dichalcogenides (TMDs), hexagonal boron nitrides (hBNs), phosphorene, germanene etc. for studying its deep root mechanism for different applications.[8]

To be more precise, a multilayered hexagonal MXenes with versatile properties, have been synthesized from the layered ternary material - $M_{n+1}AX_n$ (termed as MAX phase). MAX phase is etched to create materials such as 2D metal carbides, nitrides, and carbonitrides, for both LIBs and NIBs. The selective etching of 'A' layer generally give rise to the formula $M_{n+1}X_nT_x$ where, 'M' is transition metal, 'A' is from group IIIA or IVA, 'X' is the carbides, nitrides or carbonitrides and 'T' represents the surface terminations formed during the etching process.[9,10] So far, more than 60 materials have been reported for the MXene family and still research is continuing. MXenes does not possess evident precursors in nature, instead they are chiefly prepared by wet chemical etching of the corresponding MAX phase materials. It has a layered hexagonal structure in which M–X and M–A bonds have stronger interaction, where MX layers are stacked hexagonally and the 'A' atomic layers are along the c-axis.[11] In general, there are two distinct types of approaches for synthesis (i) top-down, in which exfoliation of few layers from the bulk and (ii) bottom-up, a deposition-based growth of material.[12] The unique compositions and characteristics like larger surface area, interlayer spacing, surface terminations, excellent electrochemical performances and ideal energy accord the application in both LIBs and NIBs.[13] A wide range of organic molecules, nanoparticles, and mono- and multivalent cations may fit inside the interlayer gap in MXene because of its favorable 2D stacking.[14] The highly ordered structure of MXene

[a] A. V Nair, D. S. Baji, S. Nair, D. Santhanagopalan
Amrita School of Nanosciences and Molecular Medicine, Amrita Vishwa Vidyapeetham, Ponekkara, Kochi, India
E-mail: dsgopalan20710@aims.amrita.edu

Supporting information for this article is available on the WWW under https://doi.org/10.1002/batt.202400493

Research Article
doi.org/10.1002/batt.202400493
Chemistry Europe
European Chemical Societies Publishing

allows for theoretical calculations to foresee its properties and allows for the synthesis of numerous molecules in various dimensions.[15] The quest for developing lithium and post-lithium-ion batteries with high energy density, high power density, sustainability and cost-effectiveness is still ongoing. An anode material that is suitable and has competitive electrochemical performance is a primary obstacle impeding the advancement of such technologies.[16] Here, we focused on $Ti_3C_2T_x$ though Ti_2C MXenes possess higher theoretical capacity, it is less stable due to oxidation. Secondly, the theoretical capacity of $Ti_3C_2T_x$ varies according to the lithium adsorption. For example, from theoretical capacity varies from 320 mAh/g to 447.8 mAh/g when lithium adatoms changes from 2 to 2.8 Li per formula.[17] Thus, this work is an attempt to show that MXene can be used for both LIB and NIB and discusses the surface chemical changes and the composition of the solid electrolyte interphase (SEI) layer at different stages of the charge-discharging process.

Experimental Section

This work focuses on the use of HF for wet chemical etching of the MAX phase. Certain amount of Ti_3AlC_2, HF and DI water taken in Teflon lined beaker, kept for stirring at room temperature for 15 hours. After the process, centrifuge the materials to neutralize and is then kept for drying at 80 °C for 12 hours. The resultant MXene contains dangling bonds and surface terminations like –OH, -O and –F.[18] To eliminate the surface terminations mainly hydrating bonds, the resultant product undergoes annealing at a different temperature like 250 °C and 500 °C for 3 hours at 5 °C/minute in Argon atmosphere. Hereafter, the samples were named as commercial sample as TCT-Com, unannealed sample will be TCT, annealed at 250 °C will be TCT-250 and annealed at 500 °C will be TCT-500. The samples were subjected to X-ray diffraction (D2 Phaser, 2nd generation, Bruker, Germany, the Cu $K\alpha_2$ signals and background subtraction of the data were performed using EVA™ program provided by Bruker) and transmission electron microscopy (TECHNAI, FEI, The Netherlands) to assert structural and microscopic information. To test the electrochemical performance four slurries were made with samples as active material, CNT and PVDF as conductive material and binder were taken in a ratio of 70:15:15 with NMP as solvent. It is casted on top of a copper foil and dried in a lamp oven of temperature 80 °C, for 15 minutes. Swagelok cells were made with a loading of the order of 1.0 mg/cm^2, inside the glove box (< 1 ppm O2 and H_2O), using commercial 1 M $LiPF_6$ in EC: DMC as electrolyte for LIBs and homemade 1 M CF_3NaO_2S (Sodium Triflate) in 2-Methoxyethyl ether (or Diglyme) solvent as electrolyte for NIBs. The electrochemical testing was carried out in BCS-805, Biologic Instruments in the voltage window of 0.01–3.0 V. For Ex situ XPS purposes the half-cells (half-inch Swagelok cells) were assembled and electrochemical cycled to the respective voltages (charge/discharge) of 1.0, 0.5 and 0.01 V during discharge and 1.5 and 3.0 V during charge. Subsequently, the cells were taken inside the glove box disassembled, the electrode was washed with the respective solvent and kept for drying inside the glove box before loading in to the XPS chamber (Kratos, UK) for analysis. During the transfer process, the electrodes were briefly exposed to atmospheric conditions. Electrochemical impedance spectroscopy (EIS) analysis were carried out in the form of LIB and NIB half-cells for TCT-500 electrodes. The ac amplitude was fixed at 50 mV while the data was collected for a frequency range of 10 mHz to 100 kHz during 1st charge/discharge cycle at predetermined voltages consistent with the ex situ XPS data.

Result and Discussions

Figure 1 represents the XRD data for $Ti_3C_2T_x$ MXene samples including as etched, 250 °C and 500 °C annealed. The as prepared TCT sample XRD exhibit minor impurities which is consistent with that of the literature.[19,20] It may be noted that the TCT sample exhibit most intense peak at a 2θ value of 7.2° while a low intense peak at 9.3°. The intense peak corresponds

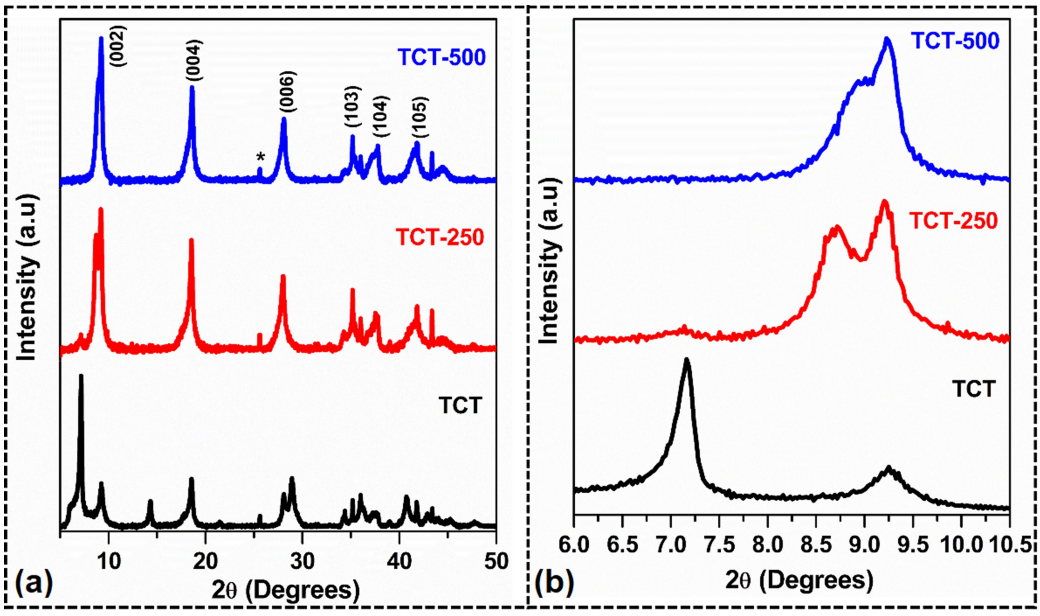

Figure 1. (a) XRD representation of TCT, TCT-250 and TCT-500 and (b) magnified view of (002) peak of TCT, TCT-250 and TCT-500.

Research Article
doi.org/10.1002/batt.202400493
Chemistry Europe
European Chemical Societies Publishing

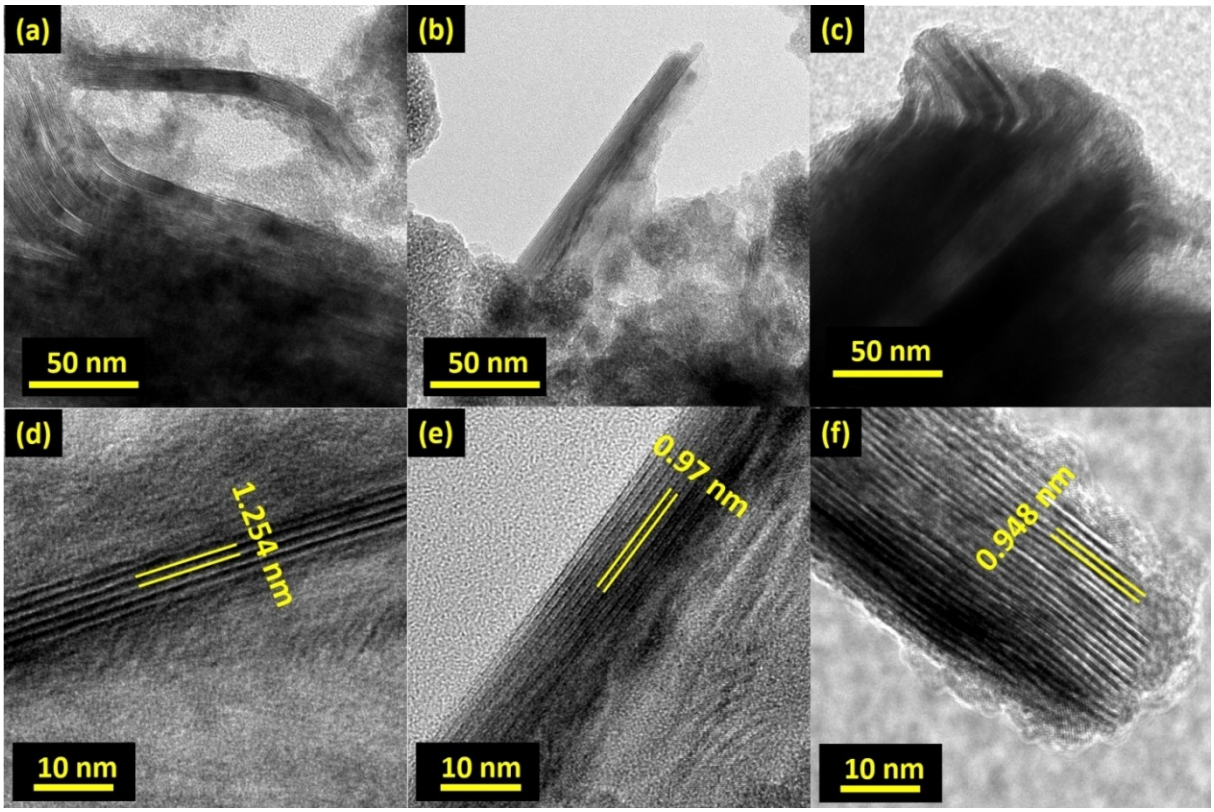

Figure 2. Low (a-c) and high (d-f) resolution TEM images of TCT, TCT-250 and TCT-500 respectively.

to surface terminations involving F^- and OH^- and the minor peak indicates dehydrated TCT. It may be noted that the annealed samples TCT-250 and TCT-500 shows intense peaks at 9.3° indicating OH- removal during thermal treatment and hence lattice contraction. A magnified view in Figure 1(b) of the (002) peak has a doublet that possibly correspond to O^{2-} in place of OH^-. Also, a minor peak indicated by * appeared around 26° could be Al_2O_3/TiO_2.

For the microstructure study, TEM analysis was employed. Here, the TCT sample exhibit 1.254 nm d-spacing compared to the annealed samples of 0.97 nm and 0.948 nm for TCT-250 and TCT-500 respectively. It is clear that the 2D structure flakes inter-layer spacing are altered after thermal treatment due to the OH^- termination removal. It is established that TEM and XRD results are consistent as a function of temperature.

Further the powder samples were subjected to XPS analysis and Figure S1 shows the survey scans of all the three samples indicating no impurity elements are present. Figure 3 depicts the XPS representation of synthesized TCT, 250 °C and 500 °C annealed TCT samples. In the C 1s spectra (Figure 3a) three peaks were identified at 281.1, 284.8 and 288.7 eV for TCT, 281.05, 284.6 and 288.3 eV for TCT-250 and for TCT-500 281.1, 284.6 and 288.7 eV with some peak shifts. The peaks are related to respective compounds like C–Ti, C–C and O–C=O. Among this C–C has the highest for all three samples and it can be seen that carbonate bond O–C=O bond is decreasing annealing at higher temperatures which actually concluding that oxygen content becoming very less as annealing at higher temperature in the inert atmosphere. For O 1s spectrum (Figure 3b) binding energy ranges between 529.8 and 530.1 eV is attributed to Ti–O and Ti–O–Ti bonds along with a new peak at 531.5 eV which is only for TCT-500 sample which is the formation of Ti–OH bond. The formation of F 1s is strictly from the synthesis which is consistent for TCT and TCT-250 annealed sample, at 684.45 and 684.1 eV. For 500 °C annealed sample, formation of a doublet is obtained which may be due to fluorine attached as terminator (Figure 3c). The Ti 2p spectra has mainly three peaks in which after annealing the peak at 454.7–455.1 eV range Ti–C getting reduced which is because after etching it might be attached more to the surface terminations rather than Ti–C. At 458 eV Ti attains stable configuration of Ti^{4+} which is consistent with the three samples. In addition to this, formation of TiO_2 which is expected from the XRD however, for the annealed samples, the intensity of this peak reduced (Figure 3d).[21,22]

Electrochemical Studies

The galvanostatic study employed to study the performance and capacity of commercial and synthesized MXene samples for both LIB and NIB. Figure S2 (a) is the rate study of commercial TCT sample for LIB conducted at 50, 100, 250, 500 and 50 mA/g in which the resultant capacities were 267, 207, 170, 139 and 200 mAh/g respectively. Figure S2 (b) is the charge-discharge profile of TCT-Com in which first charge and discharge was 316 and 850 mAh/g, with an initial columbic efficiency (ICE) of 37 %.

Research Article
doi.org/10.1002/batt.202400493
Chemistry Europe
European Chemical Societies Publishing

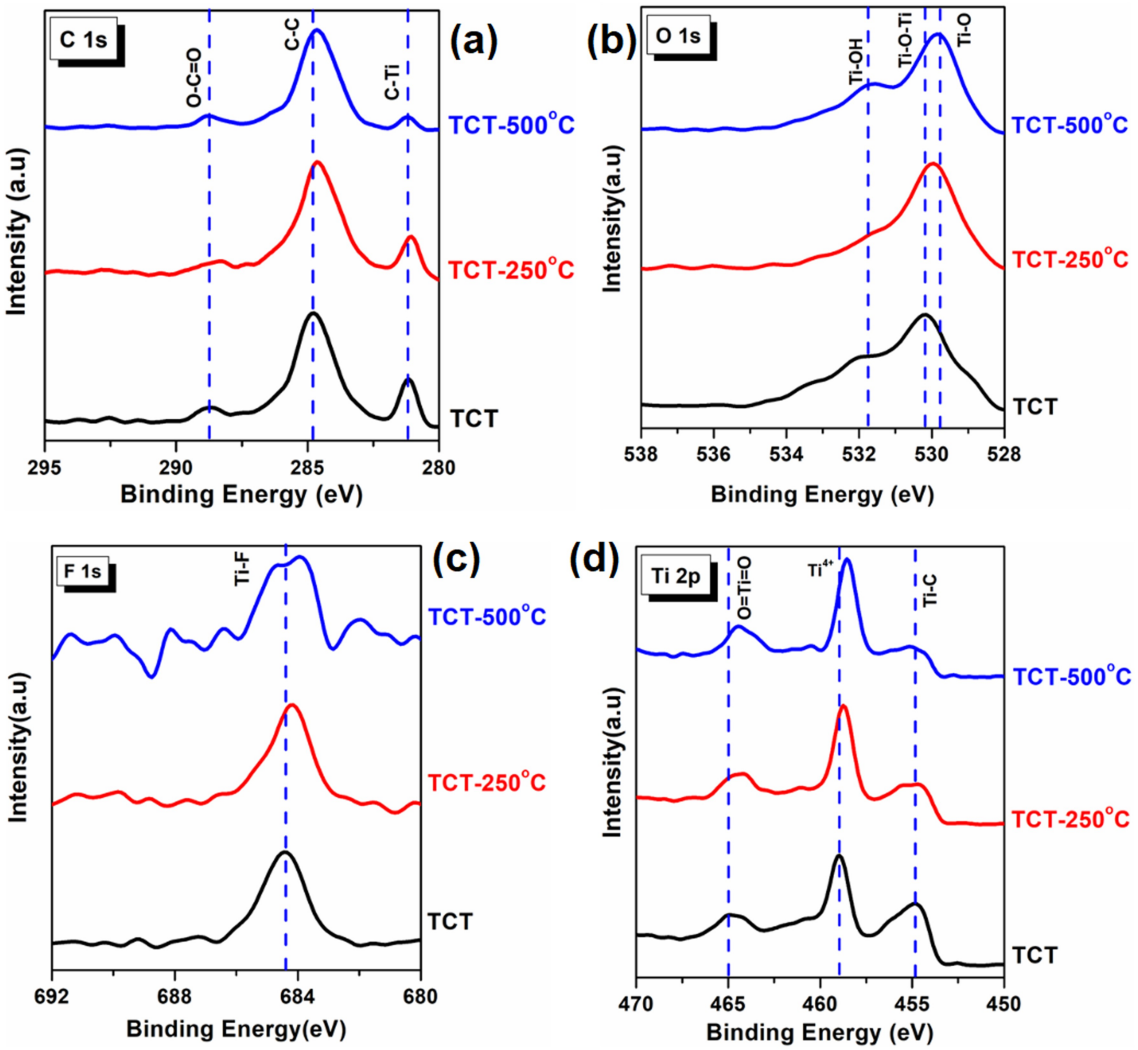

Figure 3. XPS representation of TCT, TCT-250 and TCT-500 powder samples (a) C 1s, (b) O 1s, (c) F 1s and (d) Ti 2p.

The charge capacity of long cycling at 500 mA/g for 1000 cycles was 136 mAh/g with a retention capacity of about 87%.

Figure 4 is the electrochemical performance comparison of the three samples, TCT, TCT-250 and TCT-500 for LIBs. From the rate test study, Figure 4(a) among the three at lower rates TCT performed better with a capacity of 218 and 175 mAh/g at 50 and 100 mA/g but at higher rates, 250 and 500 mA/g TCT-500 shows slightly higher capacity of 147 and 125 mAh/g. From Figure 4(b), the first discharge capacities were 593.1, 408.6 and 474.9 mAh/g for TCT, TCT-250 and TCT-500. Among that TCT-250 and TCT-500 has better ICE of 42% and 40% compared with TCT (35.8%). Figure 4(e) is the cycling performance of all the samples, in which they were cycled at 500 mA/g for 1000cycles. From the data TCT-500 has good stability and capacity as compared to the other samples. The charge capacities of three samples at 1st, 500th and 1000 cycles were 102.8, 85.7 and 67.3 mAh/g for TCT, 95.4, 91.4 and 105.2 mAh/g for TCT-250 and 128, 141.2 and 146.3 mAh/g for TCT-500. They possess a retention capacity of 65.4% for TCT, 110% for TCT-250 and 116% (activation enhanced capacity) for TCT-500. The Coulombic efficiency (CE) for all the three samples for 1000 cycles is displayed in Figure S4, which clearly shows that all the samples exhibit values between 99 and 99.7%.

In parallel, the rate testing is also conducted for NIB. The rate performance study of commercial TCT NIB comparing with LIB is very poor since at 50 mA/g itself it shows variations (Figure S3). The initial charge capacity was 283 mAh/g at 50 mA/g with reversible capacity of 154 mAh/g. At higher rates it delivers only 81.2 mAh/g with a retention of 28.6%. The initial charge capacities at various current rates are 140 mAh/g at 100 mA/g, 103.5 mAh/g at 250 mA/g and 76.9 mAh/g at 500 mA/g. The ICE is also very poor, delivers only 26%. Figure S3 (c) is cycling the sample at 500 mA/g for 500 cycles, in which it has stability issues delivers about 31.6% columbic efficiency. From Figure 5(a), describes the rate test study of TCT, TCT-250 and TCT-500. Within the samples, both TCT-250 and TCT-500 have similar kind of performances with compactable variations. Among the three TCT is performing the worst with charge capacities of 130, 106, 86 and 72 mAh/g at lower to high current rates. The first discharge capacities of each sample were

Research Article
doi.org/10.1002/batt.202400493
Chemistry Europe
European Chemical Societies Publishing

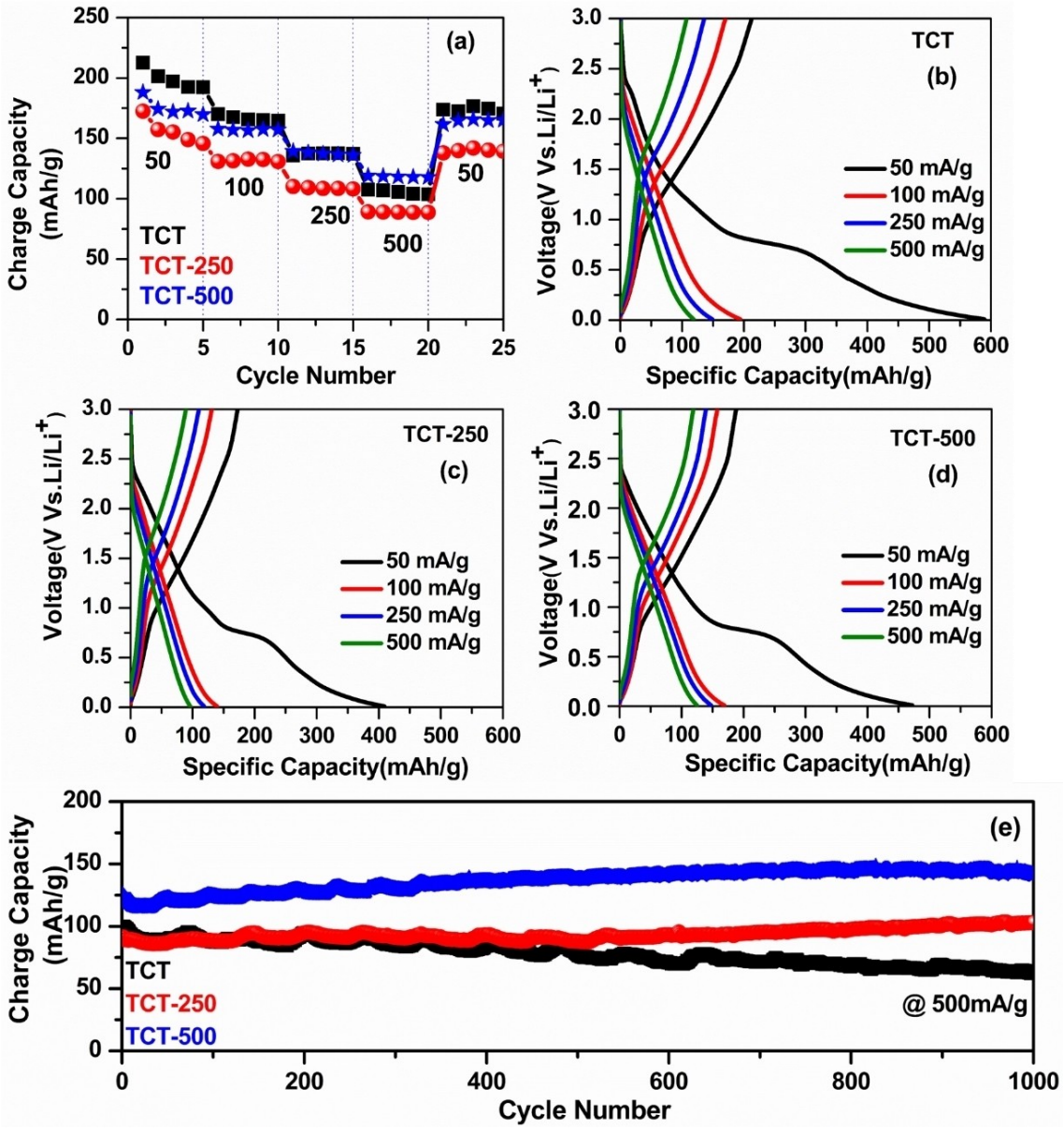

Figure 4. Electrochemical studies of TCT, TCT-250 and TCT-500 in which (a) rate performance, (b–d) charge-discharge profiles and (e) long cycling at 500 mA/g of LIB.

416.4 mAh/g for TCT, 358.08 mAh/g for TCT-250 and 378.5 mAh/g for TCT-500 observed from Figure 5 (b), (c) and (d). Thereby the ICEs were 31%, 37% and 34% for TCT, TCT-250 and TCT-500 respectively. Figure 5 (e) is the long cycling data of NIB at 500 mA/g in which the capacities at first and 1000th cycles were reported as for (i) TCT- 67.2 and 73.8 mAh/g with retention of 73.8%, (ii) TCT-250–89.6 and 57.4 with retention capacity of 64% and (iii) TCT-500 has 88.9 and 68.1 mAh/g with retention capacity of 76%. From the analysis, TCT-250 has an increase initially which gradually reduces after 250th cycle while TCT-500 exhibits an ICE of 34% with a good retention capacity of 76% higher than other two samples. Figure S5 shows the CE values for 100 cycles which is in the range of 99–99.5% for all three samples. For both LIBs and NIBs, at initial stages TCT-500 sample exhibit a lower capacity at low rates compared with the other samples. However, for the long cycling tests it is evident that at a rate of 500 mA/g the capacity of TCT-500 sample was higher compared to the other two samples for both LIB and NIB. Hence it can be concluded that due to the removal of hydroxyl terminations help in lattice contraction leading to improvement in capacity and cycling stability. Table S1 displays the performance comparison of $Ti_3C_2T_x$ samples reported in the literature[23–31] along with the results of the present work. It may be noted that long cycling in these hydroxyl termination removal played a significant role and in general initial CE values are of the order of 50% and hence improvement in initial CE value is necessary for MXene-based materials for both LIB and NIB applications. It may be noted that the electrochemical performance of LIB and NIB cells in terms of capacity, rate capability and cycling stability has been significantly better for

Research Article
doi.org/10.1002/batt.202400493
Chemistry Europe
European Chemical Societies Publishing

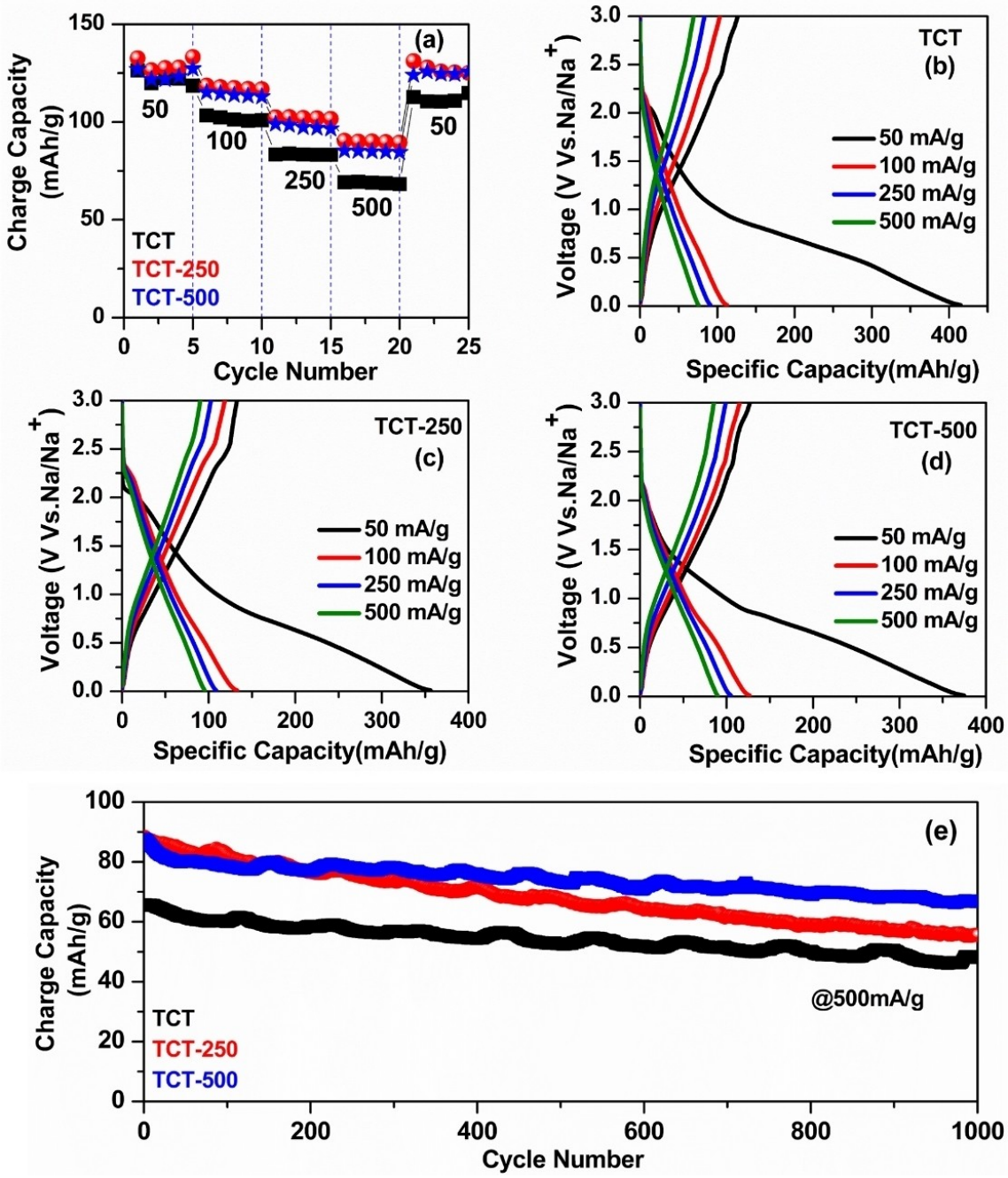

Figure 5. Electrochemical studies of TCT, TCT-250 and TCT-500 in which (a) rate performance, (b–d) charge-discharge profiles and (e) long cycling at 500 mA/g of NIB.

TCT-500 with the lowest inter-layer spacing recorded based on XRD and TEM. These results indicate that expanded inter-layer spacing does not always help in high storage capacity or rate capability.

To investigate surface chemical changes on the best performing TCT-500 electrode, *ex situ* XPS spectra were recorded and analyzed at different stages of charge/discharge. TCT-500 electrodes, discharged to different cut-off voltages of 1.0 V, 0.5 V and 0.01 V also charged to two different cut-off voltages of 1.5 V and 3.0 V for both LIB and NIB. Along with these ex situ electrodes a pristine electrode was also subjected to XPS analysis for comparison. Figure S6 (a) displays the survey spectra of the TCT-500 electrodes at different stages of lithiation/delithiation (based on the voltage). All the significant peaks in the survey spectra could be correlated to the elements present on the surface. From the XPS representation of half-cell LIB in Figure 6 (a), it can be clearly visible that bare electrode has a peak at 284.6, 286.5 and 290.9 eV corresponding to C–C, C–O and CF_2/O–C=O bonding which consistent for most of the samples along with C–Ti–O at 283.6 eV for 1.5 V cycled sample. During discharging from 1 V to 0.01 V, 0.5 V can be assumed as an intermediated stage, because most of peak merges and

Research Article
doi.org/10.1002/batt.202400493
Chemistry Europe
European Chemical Societies Publishing

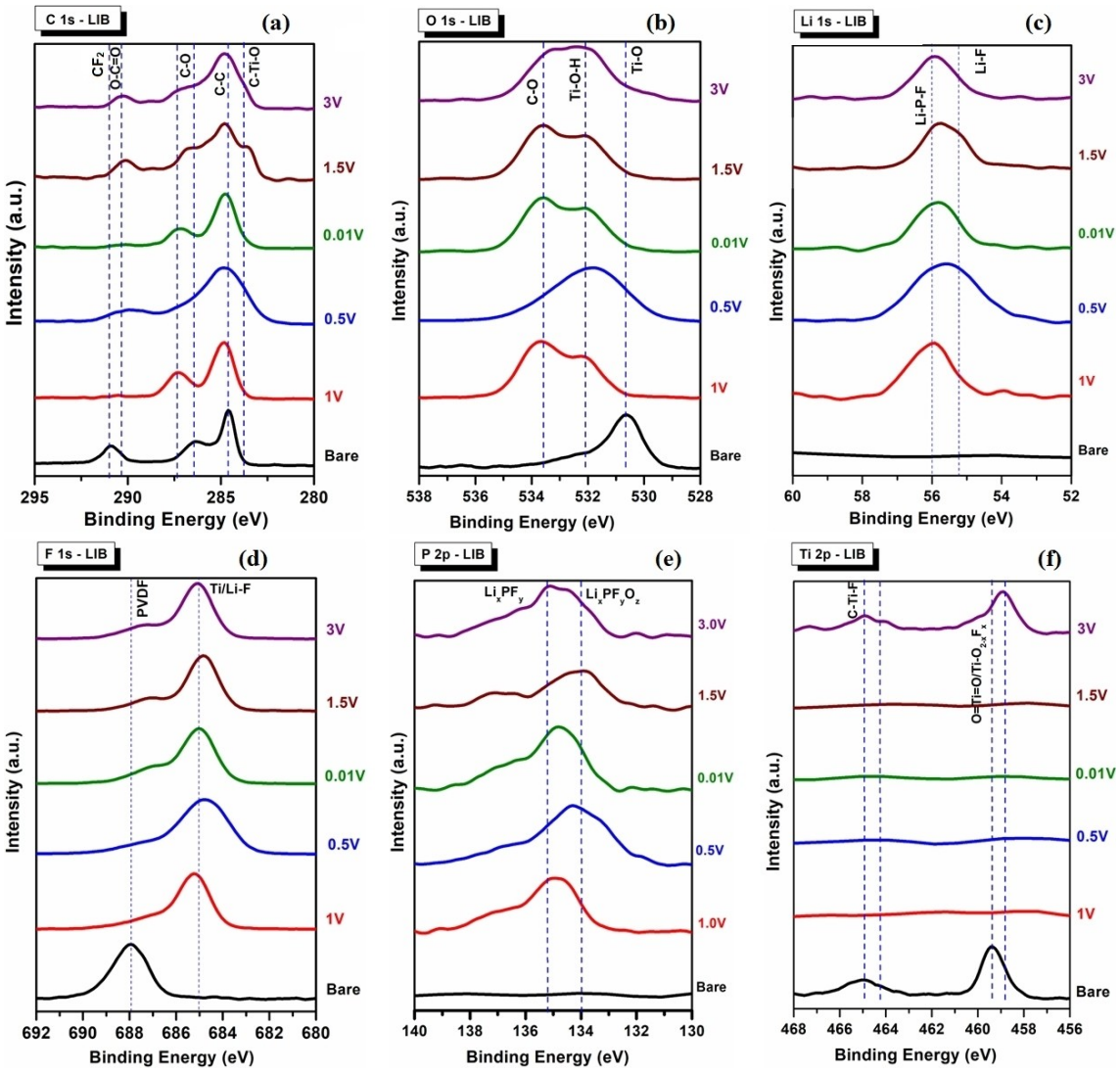

Figure 6. XPS spectrum of NIB electrodes discharged at different voltages including bare in which (a) C 1s, (b) O 1s, (c) Na 1s, (d) F 1s, (e) P 2p and (f) Ti 2p

broadens after or before this stage. The C=O peak vanishes when discharged at minimum but still exist C–C and O–C=O which could be because the formation is happened due to SEI layer and it might be masked C=O. The carbonates bond is emerging at higher discharge rates which might be due to the strong kinetics between electrode and electrolyte happened during lithiation process. It is also visible that the 0.5 V spectra (intermediate stage like 1.0 V) is broadening owing to the fact that during lithiation hydrated peak (Ti–OH) take shape rather than Ti–O. Comparing with C 1s spectra of Figure 3, all the peaks were present in the cycled samples even though SEI masked some peaks. From O 1s XPS data, bare sample at 530.65 eV exists the Ti–O peak which vanishes or else merged during discharging. At 532 eV Ti–O–H is formed, which indicates good wettability of the material is observed, which is absent in pristine but except the intermediate stage all other voltages it exists and is formed by charging/discharging at SEI layer. In addition, presence of Ti–O bond even in bare sample evidences the confirmation of TiO_2 but during cycling at different voltages this oxidation is inhibited by interfacial self-assembly process. The pristine oxides after cycling are hydrated and forms Ti–O–H bond.[32,33] In Li 1s bare sample has no peaks for Li–P–F and Li–F so hence we can draw a conclusion that these peaks are formed only during cycling process. As cycling progress, Li–F merges to Li–P–F which is consistent and might be formed due to the intercalation/de-intercalation of Li-ions. From F 1s XPS analysis in figure, the pristine sample has fluorine peak only at 688 eV which is formed from the binder used for slurry casting. After cycling, at 685 eV Ti/Li–F (metal fluoride) bond is formed and is consistent for all the cycled samples. Also, the PVDF peak is diminishes at lower voltages during discharging/charging process. From Figure 6, P 2p data, emerged from the electrolyte used so will be absent in pristine sample. At 134 eV $Li_xPF_yO_2$ and 135.1 eV Li_xPF_y peaks exists with some shifts. This is mainly because of the hydrolysis of electrolyte happens in the hygroscopic material, thereby decomposition of carbonate occurs.[34–36] At stable states the shift observed towards higher potential. As the SEI layer

Research Article
doi.org/10.1002/batt.202400493
Chemistry Europe
European Chemical Societies Publishing

progresses during discharging the peak becomes more specified. On the other hand, charging progress the peak broadens. Due to electrolyte-SEI layer combination, oxides are also formed mostly at stable configurations. Finally, from the Ti 2p representation in the figure, no peaks were formed in between voltages except for bare and at end of charge (delithiation). The Ti $2p_{3/2}$ peaks are broad possibly due to convolution, especially peaks at 458.9 and 459.1 eV correspond to O═Ti═O/Ti–$O_{2-x}F_x$ no clear signatures of Ti–C was observed. From the powder data in Figure 3, the peaks formed almost consistent with titanium having mixed oxidation states of Ti^{4+} and Ti^{3+}. Hence it may be noted that the changes happen in Ti obscured below the SEI layer but when charged to 3.0 V the Ti signals are visible (indicating a possible reversibility/dissolution of the SEI layer). While comparing bare and charged to 3.0 V data, the intensity of Ti 2p is less but visible compared to other stages of charge/discharge due to SEI layer formed upon cycling.[37] The SEI layer is so thick at all intermediate stages of lithiation/delithiation that the Ti 2p signal is not visible. Based on the observations, the SEI layer on the surface of TCT-MXene is significant (i.e. thicker) and it showed compositional fluctuations. First during discharge up to 1.0 V, the SEI layer was of C–C/C–O organic composition and $Li_xPF_yO_z$ rich with less LiF inorganic composition. Further discharge to 0.5 V led to C–C/O–C═O rich organic composition and more LiF than $Li_xPF_yO_z$ inorganic composition was observed. At the end of discharge (0.01 V) the SEI layer was C–C/C–O organic composition and Li_xPF_y rich inorganic composition. During charge for both 1.5 V and 3.0 V the CF_2 from binder was visible along with C–C/C–O/O–C═O organic composition with Li_xPF_y rich inorganic composition with minor concentration of $Li_xPF_yO_z$. Overall, the SEI layer was a mixture of LiF/$LiF_xP_yO_z$ rich inorganic layer and C–C/C–O dominant organic layer and the results indicate that the organic layer seems to dissolve at the end of charge.

Figure S6 (b) shows the survey spectra of the TCT-500 electrodes at different stages of sodiation/desodiation (based on the voltage). All the significant peaks in the survey spectra could be correlated to the elements present on the surface. Figure 7 is the XPS analysis of NIB cells cycled at different voltages from 0.01 V–3.0 V. In the figure, C 1s before cycling the

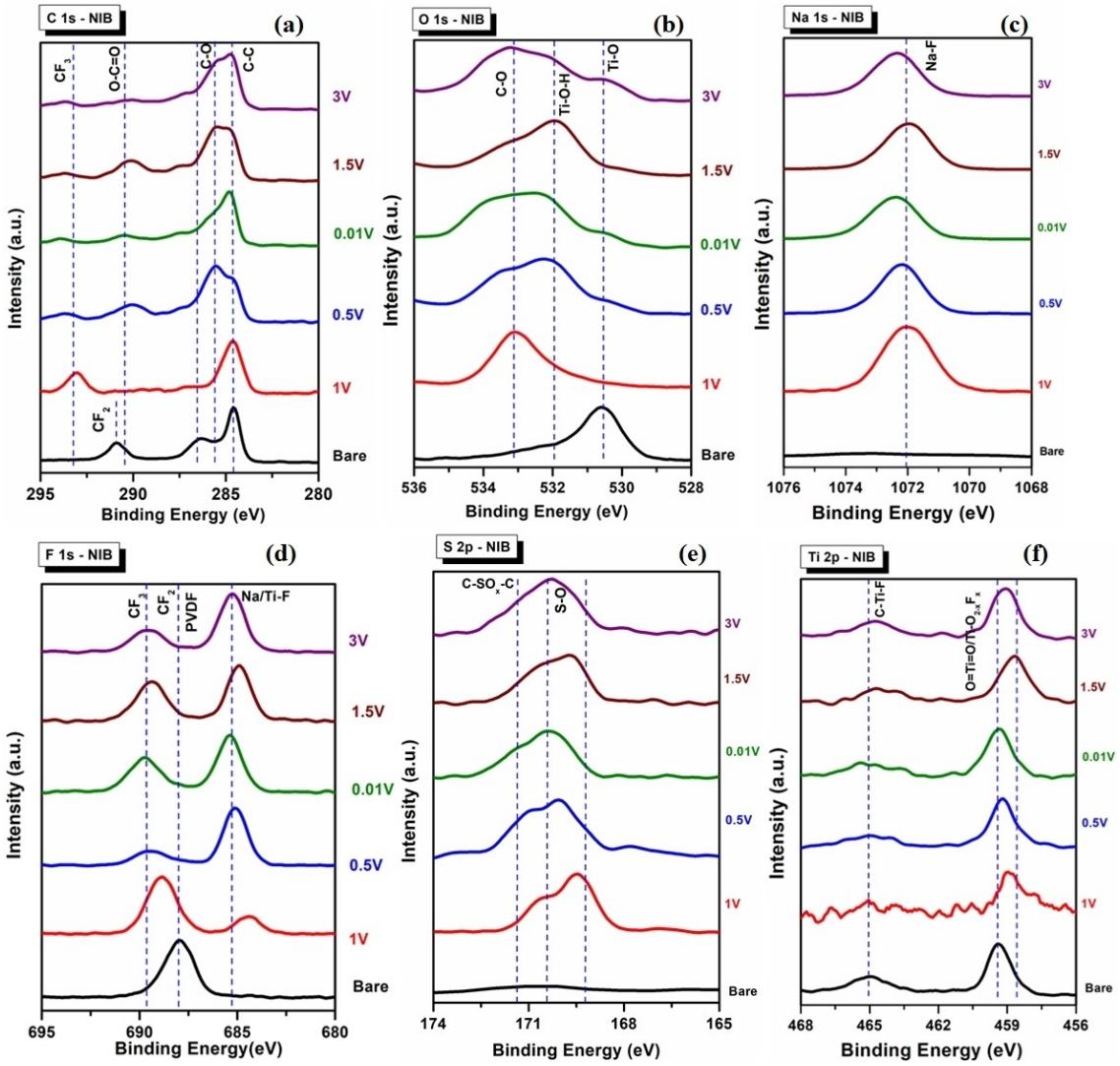

Figure 7. XPS spectrum of NIB electrodes discharged at different voltages including bare in which (a) C 1s, (b) O 1s, (c) Na 1s, (d) F 1s, (e) S 2p and (f) Ti 2p

main peaks obtained 284.6 eV for C–C, 286.5 for C–O and 290.9 eV for O–C=O which is agreeing with the powdered samples done before (Figure 3). It has been noticing that the high intensity C–C bond still present but the C–O diminished discharged to lower voltages similarly O–C=O has variations with voltages which may be due to bonding happened with electrolyte and SEI layer formed. Mostly the oxygenated bonds get lessen so it might be inhibited and new peak at 293 eV attributing to $C–F_3$ so the surface termination bonding becomes stronger than oxygen containing bonds. From the O 1s spectrum, the main peak in the bare sample was at 530.7 eV for Ti–O rest all other peaks were randomly shifted. At 0.01 V and 0.5 V the bond present were Ti–O at 530.4 eV (low intensity) and broad peak at 532.9 eV Ti–OH. But at 1 V the nature of the sample is different it has only C–O bond at 533.1 eV. For higher potential 3 V, retention of Ti–O, and Ti–OH were found it could be due to the reactions occur at surface because of sodiation/ desodiation. Also, when comparing with powdered samples Ti–OH peak was new which raised by the intercalation with electrolyte. Hence it can be concluded that the SEI layer formed at very low voltages when charged at 1.5 V–3.0 V dissolves and it starts regain to the pristine. So, there is a possibility to site that equal number of intercalation and de-intercalation of sodium ions. The Na–F peak is formed at 1072 eV is because of the interaction between Na and electrolyte which contains fluorine. At low and high voltages, it shows a slight shift from other samples which may be due to formation/dissolving of SEI layer. For pristine sample the main peak was at 687.95 eV assign to the binder-electrode contact. When the sample is cycled the oxidation state of fluorine varies between $+2$ to $+3$ which may be improves the kinetics of ions between electrodes. The counter factor in this data is that except for 1 V and bare, all others have similar spectrum. The strong electrolyte interaction is visible from the spectrum because C–F bond is formed only from the electrolyte used which also plays crucial role in sodiation/ desodiation. The S 2p in the figure has main peaks for sulfate and sulfonate groups (SO_4 and C-SO_x) between 169.5–170.5 eV and 170.5–171.4 eV. It is clear that S 2p is also formed between the electrolyte- sample association, in which every sample contains both the peaks which is merged.[38,39] The Ti 2p spectrum impart that both bare and cycled electrodes exhibit similar peaks except a peak shift to lower binding energy indicating a charged interaction of C–Ti–F at certain voltages especially, during charging (desodiation). Ti peaks are analyzing in which presence of Ti^{3+} is very much low as compared to Ti^{4+}. The pristine sample had defined peaks better than the cycled samples.

Based on the observations, the SEI layer on the surface of TCT-MXene is thin and stable with minimal fluctuations in the inorganic component while the organic component was still fluctuating but less compared to Li-counterpart. First during discharge up to 1.0 V, the SEI layer was of C–C/C–O with reasonable C–SO_x–C and CF_3 concentration (from the electrolyte salt) of organic composition and NaF rich inorganic composition. Further, discharge to 0.5 V led to C–C rich and minor O–C=O component of the organic composition and NaF rich SO_x (possibly metal sulfate) inorganic composition was observed. Also, charged interactions of C–Ti–F and Ti–O–H induced peak shifts to higher binding energy overcoming Ti^{3+} reduction was observed. At the end of discharge (0.01 V) the SEI layer was C–C/C–O, CF_3 rich and minor C–SO_x–C organic composition and NaF rich inorganic composition with Ti 2p shifting to higher binding energy was observed. During charging up to 1.5 V, CF_3 and C–SO_x–C from electrolyte decomposition was still observed along with C–C/C–O/O–C=O as the organic composition. The O–Ti–F and Ti–O–H components were high which led to a shift to lower energy interaction was strong leading to a shift of Ti 2p to lower binding energy overcoming the high energy shift due to desodiation. It seems that 1.5 V charged electrode was relatively more surface sensitive (especially to atmospheric exposure during transfer to XPS chamber). Upon complete desodiation (end of charge 3.0 V), C–C/C–O were dominant with significant SO_x and Ti 2p shifting completely to Ti^{4+} and Ti–O–H intensity decreased. Inorganic NaF concentration on the SEI layer was high at the end of charge (desodiation). Overall, the SEI layer thickness on Na-ion cycled electrodes is less on the electrodes compared to the thick SEI layer for lithium counterpart (which could be due to glyme-based solvent for sodium and carbonate-based solvents for lithium electrolyte). The SEI layer is NaF rich inorganic layer while CF_3, sulfonate and C–C/C–O dominant organic layer due to the salt and solvent decomposition.

To understand the electrode properties and the kinetics between electrode-electrolyte along with SEI layer during charge-discharge, electrochemical impedance spectroscopy studies were carried out. At pre-determined voltages consistent with the ex situ XPS to be able to get a correlation for TCT-500 both LIB and NIB half-cells. The charge transfer resistance (R_{ct}) and system resistance (R_s) were investigated and correlated with ex situ XPS results. The complete EIS data is provided in the Figure S7 while magnified view of the data corresponding to the semicircle region in the following discussions.

From Figure 8, the spectrum recorded at open circuit voltage (OCV) condition shows single semicircle with R_s and R_{ct} values provided in the Table S2, while the next 3 set of EIS data recorded during discharge clearly shows two semi-circles with the semicircle in the high frequency region correspond to SEI layer resistance (R_{SEI}) confirming the SEI layer formation consistent with the ex situ XPS results. As the lithiation increases (deep discharge), initially the charge transfer resistance increases compared to the OCV condition subsequently, decreases though not below the OCV condition R_{ct} value. While the SEI layer resistance did not change significantly (Table S2) indicates that the uniform and stable SEI layer with no appreciable composition variations. The major change was at 1.0 V consistent with the ex situ XPS results. During charging, the one of the semicircle almost vanished with R_{ct} values well below the OCV condition values indicating possible dissolution of some component of the SEI layer as noted from the minor compositional changes of the SEI layer in XPS results. It may be noted that in LIB system with reduction induced higher diffusion, low internal resistance and low charge transfer resistance indicates a uniform SEI layer leading to improved performance.[40]

Research Article
doi.org/10.1002/batt.202400493
Chemistry Europe
European Chemical Societies Publishing

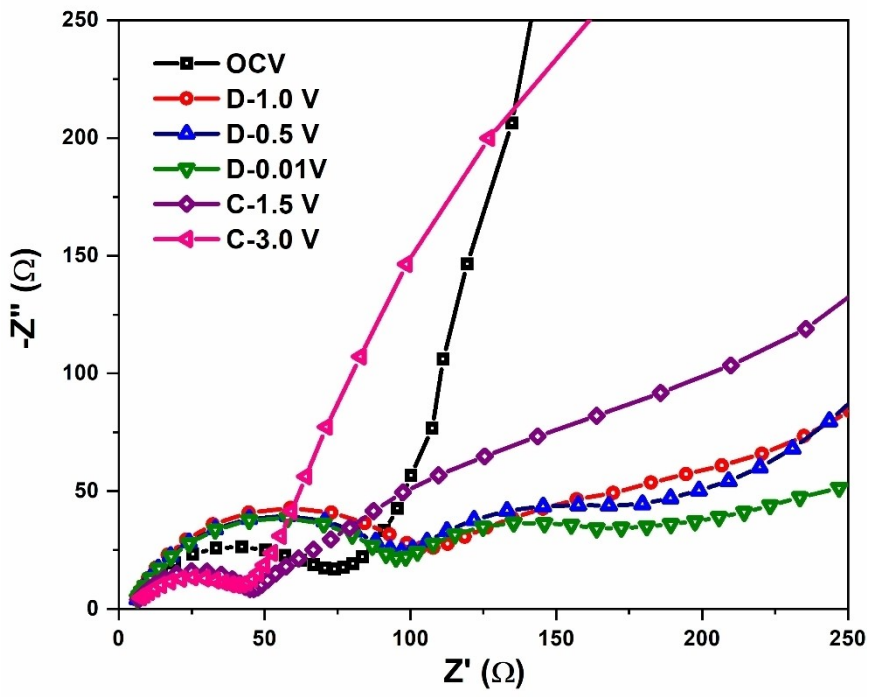

Figure 8. EIS spectra of TCT-500 at different pre-determined voltages for LIB

In the Figure 9, similar to LIB, EIS for NIB was also conducted. The R_s values were similar for all the samples and also comparable with the LIB systems. However, the R_{ct} values were significantly lower in the range of 40 to 20 Ω during discharge, which is consistent with the thin SEI layer observed with the XPS results which is attributed to the glyme-based electrolyte. Also the semicircle induced by the SEI layer was also not observable, possibly the time constant of the diffusion though the SEI layer and the charge transfer process are similar. During charging the R_{ct} value increased with end-of-charge and OCV condition values were similar indicating a consistent surface with thin SEI layer without performance issues for NIB

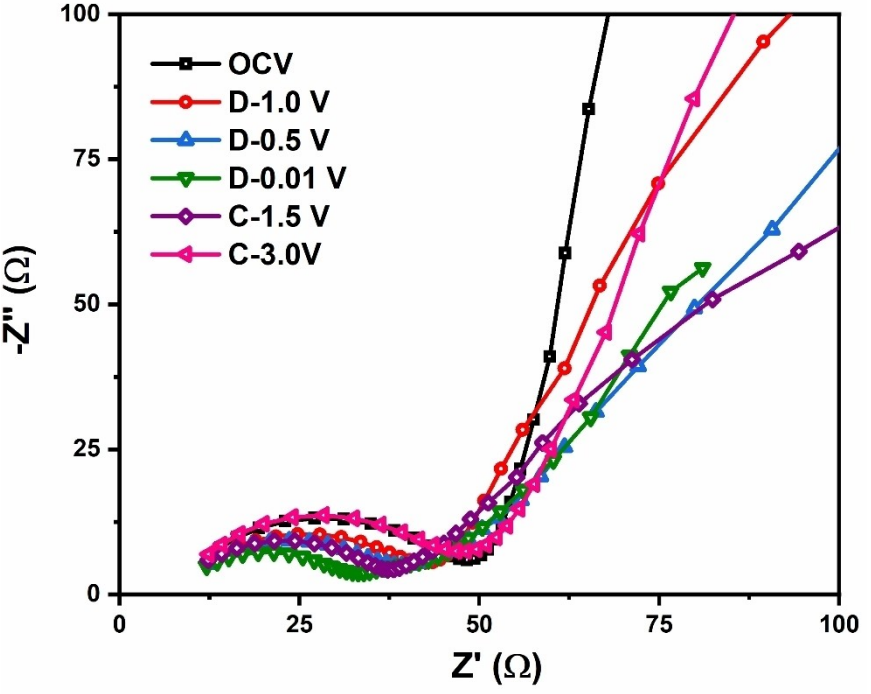

Figure 9. EIS spectra of TCT-500 at different pre-determined voltages for NIB

as well. Thus, a strong interaction of electrode-electrolyte and with the transition metal is visible along the XPS analysis without compensating the stability and performance. As a result, the system holds low internal resistance by improving the ionic conductivity.[41] From the impedance studies, the formation of stable SEI layer helps to improve the efficiency and performance of both LIB and NIB cells. For LIB due to the use of carbonates-based electrolyte, formation of thick but stable SEI layer is observed, which is consistent with the ex situ XPS results. On the other hand, in NIB the SEI layer is thin which improves the diffusion and stability by lowering the internal resistance at these specified voltages.

Conclusions

Herein the work has studied the synthesis, characteristics and electrochemical investigations of $Ti_3C_2T_x$. Initially, demonstrated an optimized synthesis of $Ti_3C_2T_x$ from its MAX phase using HF precursor which is then fabricated to lithium and sodium-ion batteries. The performance was compared with commercial and synthesized $Ti_3C_2T_x$ samples. This work proved that TCT-500 has better performance compared to commercial and other samples with an ICE of 40% for LIB and 34% for NIB. This can be improved further by surface engineering, tuning the surface terminations or compositing etc. Additionally, investigated the electrode-electrolyte interface at different stages of charge/discharge from 0.01 V–3.0 V using *ex situ* XPS. Such an in depth study to understand the surface chemical changes using XPS has not been employed yet in any literature. The carbonate and ether-based electrolytes for Li-ion and Na-ion batteries respectively exhibit significant differences in the SEI layer composition. The SEI layer thickness was significantly higher for Li-ion compared to Na-ion and the composition fluctuations was strong in Li-ion compared to Na-ion. However, the similarity was the SEI layer in both cases was mixture of organic and inorganic components. From the study of electrode-electrolyte interaction for TCT 2D materials, the formation of SEI layer is different in both Li-ion and Na-ion cells due to the use of different electrolyte solvents. As for the electrochemical performance improvements are concerned, surface termination modifications will be the critical factor. Thus, developed a 2D MXene-based material for high performance in both Li-ion and Na-ion battery applications. Also established that the kinetics are based on the reactions at electrode-electrolyte interface.

Acknowledgements

DS acknowledges the SERB, Govt. of India, for the funding (CRG/2021/004325) and fellowship for AVN. The authors also thank Amrita Vishwa Vidyapeetham for support. We thank Dr. Silpasree S J for helping with the experiments at the initial stages.

Conflict of Interests

The authors declare no conflict of interest.

Data Availability Statement

The data that support the findings of this study are available in the supplementary material of this article.

Keywords: MXene · $Ti_3C_2T_x$ · Anode · Li-ion battery · Na-ion battery · Surface chemistry

[1] J. N. Tiwari, R. N. Tiwari, K. S. Kim, *Prog. Mater. Sci.* **2012**, *57*, 724–803.
[2] E. E. Elemike, J. Adeyemi, D. C. Onwudiwe, L. Wei, A. O. Oyedeji, *J Energy Storage.* **2022**, *50*, 104711.
[3] Y. Wu, Y. Yu, *Energy Storage Mater.* **2019**, *16*, 323–343.
[4] J. Y. Hwang, S. T. Myung, Y. K. Sun, *Chem. Soc. Rev.* **2017**, *46*, 3529–3614.
[5] P. K. Nayak, L. Yang, W. Brehm, P. Adelhelm, *Angew. Chem. Int. Ed. Engl.* **2017**, *57*, 102–120.
[6] Z. Shadike, E. Zhao, Y. N. Zhou, X. Yu, Y. Yang, E. Hu, S. Bak, L. Gu, X. Q. Yang, *Adv. Energy Mater.* **2018**, *8*, 1702588.
[7] P. Vishnoi, K. Pramoda, C. N. R. Rao, *ChemNanoMat* **2019**, *5*, 1062–1091.
[8] K. Chaturvedi, V. Hada, S. Paul, B. Sarma, D. Malvi, M. Dhangar, H. Bajpai, A. Singhwane, A. K. Srivastava, S. Verma, *Top. Curr. Chem.* **2023**, *381*, 11.
[9] M. R. Kumar, S. Singh, H. M. Fahmy, N. K. Jaiswal, S. Akin, A. E. Shalan, S. L. Mendez, M. Salado, *J. Power Sources* **2023**, *556*, 232256.
[10] Y. Wu, Y. Sun, J. Zheng, J. Rong, H. Li, L. Niu, *J. Phys. Energy* **2021**, *3*, 032009.
[11] F. Ming, H. Liang, G. Huang, Z. Bayhan, H. N. Alshareef, *Adv. Mater.* **2020**, *33*, 2004039.
[12] Z. Xiao, S. Ruan, L. B. Kong, W. Que, K. Zhou, Y. Liu, T. Zhang, *Springer Chem.* **2020**, 1ed, 5–93.
[13] B. Anasori, M. R. Lukatskaya, Y. Gogotsi, *Nat. Rev. Mater.* **2017**, *2*, 1–17.
[14] M. Lu, W. Han, H. Li, W. Zhang, B. Zhang, *J. Energy Chem.* **2020**, *48*, 344–363.
[15] W. Meng, X. Liu, H. Song, Y. Xie, X. Shi, M. Dargusch, Z. G. Chen, Z. Tang, S. Lu, *Nano Today* **2021**, *40*, 101273.
[16] Z. Hong, H. Maleki, T. Ludwig, Y. Zhen, M. Wilhelm, D. Lee, K. H. Kim, S. Mathur, *J. Energy Chem.* **2021**, *62*, 660–691.
[17] M. Greaves, S. Barg, M. A. Bissett, *Batteries Supercaps* **2019**, *3*, 214–235.
[18] N. Anjum, O. A. Ekuase, V. O. Eze, O. I. Okoli, *ECS J. Solid State Sci. Technol.* **2022**, *11*, 093008.
[19] A. Gentile, C. Ferrara, S. Tosoni, M. Balordi, S. Marchionna, F. Cernuschi, M. H. Kim, H. W. Lee, R. Ruffo, *Small Methods* **2020**, *4*, 2000314.
[20] K. A. Perry, W. Straka, D. Keith, S. Han, L. Reynolds, B. Gautam, D. E. Autrey, *Materials (Basel)* **2021**, *14*, 694.
[21] B. Ahmed, D. H. Anjum, M. N. Hedhili, Y. Gogotsi, H. N. Alshareef, *Nanoscale* **2016**, *8*, 7580–7587.
[22] J. Chun, X. Wang, Y. Zhang, C. Wei, Z. Wang, J. Feng, *VAC* **2023**, *207*, 111476.
[23] D. Sun, M. Wang, Z. Li, G. Fan, L. Z. Fan, A. Zhou, *Electrochem. Commun.* **2014**, *47*, 80–83.
[24] L. Huang, T. Li, Q. Liu, J. Gu, *Electrochem. Commun.* **2019**, *104*, 106472.
[25] W. Zheng, P. Zhang, J. Chen, W. B. Tian, Y. M. Zhang, Z. M. Sun, *J. Mater. Chem. A* **2018**, *6*, 3543–3551.
[26] Q. Zhao, Q. Zhu, J. Miao, P. Zhang, P. Wan, L. He, B. Xu, *Small* **2019**, *15*, 1904293.
[27] B. Ahmed, D. H. Anjum, Y. Gogotsi, H. N. Alshareef, *Nano Energy* **2017**, *34*, 249–256.
[28] S. Kajiyama, L. Szabova, K. Sodeyama, H. Iinuma, R. Morita, K. Gotoh, Y. Tateyama, M. Okubo, A. Yamada, *ACS Nano* **2016**, *10*, 3334–3341.
[29] A. Gentile, C. Ferrara, S. Tosoni, M. Balordi, S. Marchionna, F. Cernuschi, M. H. Kim, H. W. Lee, R. Ruffo, *Small* **2020**, *4*, 2000314.
[30] Y. Wu, P. Nie, J. Wang, H. Dou, X. Zhang, *ACS Appl. Mater. Interfaces* **2017**, *9*, 39610–39617.
[31] G. Lv, J. Wang, Z. Shi, L. Fan, *Mater. Lett.* **2018**, *219*, 45–50.
[32] Z. Zou, Q. Wang, J. Yan, K. Zhu, K. Ye, G. Wang, D. Cao, *ACS Nano* **2021**, *15*, 12140–12150.

[33] L. Yao, X. Tian, X. Cui, R. Zhao, X. Xiao, Y. Wang, *J. Mater.* **2021**, *32*, 27837–27848.
[34] Y. Tang, C. Yang, M. Sheng, X. Yin, W. Que, *ACS Sustain. Chem. Eng.* **2020**, *8*, 12990–12998.
[35] I. Kallquist, R. L. Ruyet, H. Liu, R. Mogensen, M. T. Lee, K. Edstrom, A. J. Naylor, *J. Mater.* **2022**, *10*, 19466–19505.
[36] A. Mateen, M. Z. Ansari, Q. Abbas, A. Muneeb, A. Hussain, E. T. Eldin, F. M. Alzahrani, N. S. Alsaiari, S. Ali, M. S. Javed, *Molecules* **2022**, *27*, 7446.
[37] J. Vida, P. Gemeiner, M. Pavlickova, M. Mazalova, P. Soucek, D. Plasienka, T. Homola, *Nanoscale* **2022**, *15*, 1289–1298.
[38] C. Yuwen, B. Liu, Q. Rong, L. Zhang, S. Guo, *Sci Total Env.* **2022**, *817*, 152995.
[39] H. Peng, X. Wang, Y. Zhao, T. Tan, Z. Bakenov, Y. Zhang, *Polymers (Basel)* **2018**, *10*, 399.
[40] R. Cheng, T. Hu, H. Zhang, C. Wang, M. Hu, J. Yang, C. Cui, T. Guang, C. Li, C. Shi, P. Hou, X. Wang, *J. Phys. Chem.* **2019**, *123*, 1099–1109.
[41] M. Zarrabeitia, M. A. M. Marquez, F. Nobili, T. Rojo, M. C. Cabanas, *Batteries.* **2017**, *3*, 16.

Manuscript received: July 18, 2024
Revised manuscript received: September 18, 2024
Accepted manuscript online: September 24, 2024
Version of record online: November 9, 2024